# A Team Effort to Solve Strip Surface Quality Issues From Hot Rolling Critical Applications

This paper describes how the results of laboratory tests and their validation, as well as on-site investigations, enabled the development of a new roll shell material. Several tests were carried out with two different lab test configurations simulating the rolling process in a three-disc configuration (strip–work roll–backup roll). This led to the goal of suppressing orange peel formation linked to graphitic high-speed steels. Through the extensive and close collaboration between Eisenwerk Sulzau Werfen R&E Weinberger AG, R&D labs and Tata Steel, an important step was taken in the development of wear-resistant roll materials for surface-critical applications.

Authors

Michael Aigner (left), Eisenwerk Sulzau Werfen R&E Weinberger AG, Tenneck, Austria
michael.aigner@esw.co.at

Danny Beentjes, Tata Steel IJmuiden B.V, Velsen-Noord, The Netherlands

Henk Bolt, Tata Steel IJmuiden B.V, Velsen-Noord, The Netherlands

Sébastien Flament (right), CRM Group, Liège, Belgium

Armin Paar, Eisenwerk Sulzau Werfen R&E Weinberger AG, Tenneck, Austria

Leonel Elizondo, Eisenwerk Sulzau Werfen R&E Weinberger AG, Tenneck, Austria

## Introduction

The hot rolling process is a critical process in the metallurgical industry, which, among other things, affects the quality and surface finish of the rolled products. The formation of orange peel on the rolled strip is a major challenge for achieving the desired product quality. This article presents the results of extensive laboratory tests, their subsequent validation and on-site investigations that led to the development of a new roll shell material. The research focused on the formation of orange peel when using graphitic high-speed steel rolls during the rolling process. The collaboration between Eisenwerk Sulzau Werfen R&E Weinberger AG (ESW), CRM Group, universities and Tata Steel played a key role in achieving significant advances in the improvement of roll materials for surface-critical applications. Two different laboratory test configurations were used to simulate the rolling process. These configurations consist of a three-disc arrangement with a strip roll, a work roll and a backup roll to replicate the conditions that occur during the rolling process. Various parameters were systematically varied to understand the material behavior and identify the key factors that contribute to orange peel formation. The test setups simulated the conditions encountered during the rolling process and provided valuable insights into the behavior and performance of the material. In addition, a series of laboratory tests such as thermal fatigue tests were conducted to understand and mitigate the challenges posed by graphitic high-speed steels. The results of the laboratory tests were validated by on-site investigations to ensure the applicability and reliability of the developed roll shell material in real-life scenarios. The collaboration and sharing of expertise and resources enabled a holistic approach to material development, which finally led to success.

## Experimental Procedure

The flowchart serves as a road map and provides a clear and structured overview of how the various components or R&D phases are connected. Each step in the diagram corresponds to a specific action or decision and guides through the sequence of activities. In materials development, there is occasionally a point at which the desired results are not suitable, so that this path is no further pursued, as can be seen in Fig. 1.

Figure 1

**Flow diagram of Eisenwerk Sulzau Werfen R&E Weinberger AG (ESW)'s R&D process for new shell materials.**

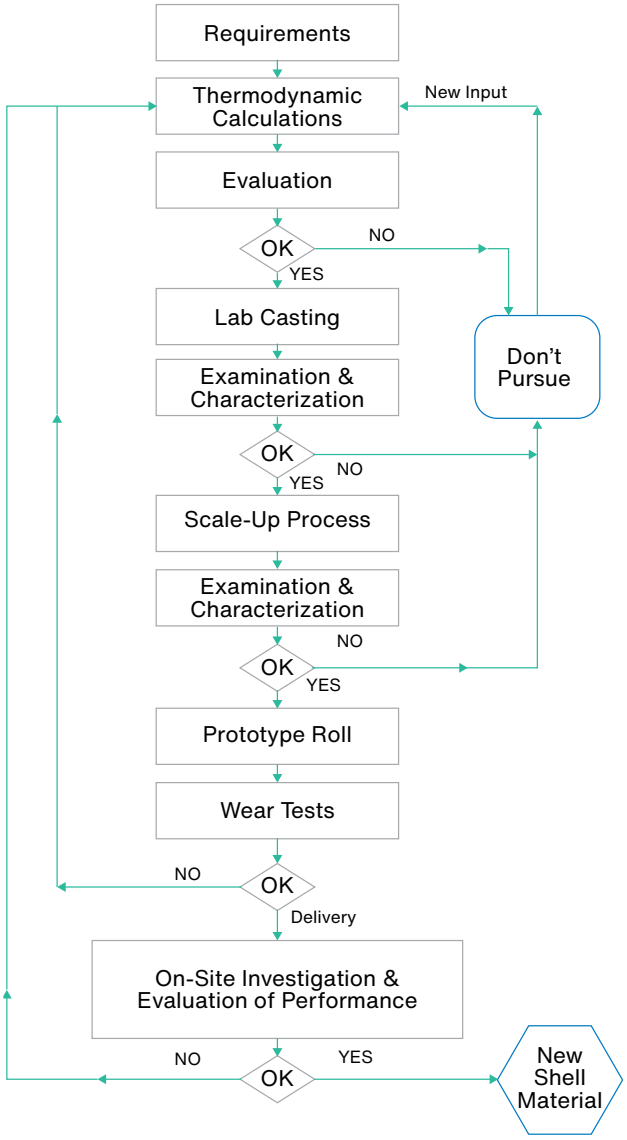


The process begins with the identification and definition of specific requirements, outlining the criteria that must be met throughout. Thermodynamic calculations are then carried out to create a numerical and theoretical basis, respectively, for the subsequent steps. Characterization steps follow, where relevant properties and features critical to the goals of the project are evaluated.

The process then moves on to laboratory casting, where the theoretical aspects are put into practice. The results of the laboratory castings are evaluated with the help of investigations and further characterization steps so that adjustments can be made, if necessary. The scale-up process is the final phase in which positive results are applied on a larger scale. The development process continues with the roll prototype, where wear tests are carried out to investigate performance under specific conditions. The investigation of the roll and the evaluation of the roll performance on-site will provide real-world insights that will validate the lab results and determine the further course of the project.

## Thermodynamic Calculations

Thermodynamic modeling of multicomponent alloys plays a crucial role in the development of different steel grades. While the application of such software to cast iron is rather limited, some studies have addressed white cast iron, as shown in previous publications.[1–3] However, the application of thermodynamic modeling for graphitic cast iron is even less common.[4]

Thermodynamic modeling of various high-alloy cast iron was carried out with Thermo-Calc 2021a and the TCFE11 database. These alloys contain carbon, silicon, and carbide-forming elements such as chromium, tungsten, vanadium and niobium. The microstructure consists of graphite, cementite and other carbides. The coexistence of carbon in carbides and graphite poses a challenge in thermodynamic calculations using the CALPHAD method.

In this project, the thermodynamic modeling was done using the chemical composition illustrated in Table 1 (all fractions given in mass %). As References 5 and 2 show a good agreement, the same phase were used to predict the alloy structure: LIQUID, FCC_A1 (austenite, MC-carbides), CEMENTITE, GRAPHITE, $M_7C_3$, $M_6C$, HCP_A3 ($M_2C$-carbides), BCC_A2 (ferrite) and $M_{23}C_6$ equilibrium calculations were performed between 1,726°C and 500°C to start from full liquid phase to a temperature where phase precipitations are very unlikely due to the low diffusion speed.

Fig. 2 shows the microstructure of Material 1, shown as a scanning electron microscopy (SEM) image recorded with a backscattered electron (BSE) detector and a magnification of 300x as well as the measured (microstructural) values. The microstructure of this material consists of a martensitic matrix with some extent of retained austenite, cementite and graphite.

Table 1

**Chemical Composition of the Investigated Material 1[5]**

| | C [%] | Si [%] | Ni [%] | Cr [%] | Mo [%] | V [%] | Nb [%] |
|---|---|---|---|---|---|---|---|
| Material 1 | 3.30 | 0.82 | 4.20 | 1.76 | 0.32 | 0.12 | 0.18 |

The equilibrium calculations for Material 1 resulted in a property diagram (Fig. 3) showing the formation of different phases at different temperatures. As suggested in Reference 5, the graphite phase was suppressed and $M_7C_3$ was considered as a chromium carbide phase. This decision was influenced by the literature reports[6,7] describing the formation of $M_{23}C_6$ as "annealing carbide" at temperatures between 650 and 780°C. In addition, Reference 5 excluded the phase BCC_A2, the body-centered cubic form (ferrite) from the calculations, as the observed microstructure is martensitic, and the martensitic transformation of the investigated materials takes place below 500°C. During the formation of the graphite phase, the amount of residual carbon is reduced. As an approximation, the residual carbon can be calculated as in Reference 5, see Eq. 1 (with: $C_{res}$ ... residual carbon; $C_{melt}$ ... total carbon in the melt; $\rho_{gr}$ ... density of graphite; $\rho_{melt}$ ... density of the melt; [%] gr ... volume percent of graphite). This means that the residual carbon must be reduced by 0.3 mass % for every volume percent of graphite.

$$C_{res} = C_{melt} - \frac{\rho_{gr}}{\rho_{melt}} * [\%]_{gr} \approx C_{melt} - \frac{2.25\left[\frac{g}{cm^3}\right]}{7.4\left[\frac{g}{cm^3}\right]} * [\%]_{gr} \approx C_{melt} - 0.3 * [\%]_{gr}$$

(Eq. 1)

The isopleth for Material 1 illustrates the impact of the reduced carbon content due to graphite formation (red line in Fig. 4). Due to the fact that the carbon content is reduced, the primary phases precipitate at higher and lower temperatures, respectively, and their fractions change which can be estimated.

Scheil-Gulliver calculations supported the decision to discard the graphite phase. The results showed that the alloy systems should be treated as white cast iron. The comparison between calculated and measured phase quantities for Material 1 showed good agreement, despite some deviations due to the suspended graphite phase. All calculations were based on these boundary conditions to predict the previously described phase types, precipitation temperatures and other relevant parameters.

## Lab Casting

The tests were carried out in an induction furnace from Junker (model MFT ST 50/3000), as shown in Fig. 5. 50 kg of the base material was molten (1). The total heat time was about 3 hours. The material was heated to approximately 1,500°C to achieve a uniform nucleation state and then cooled to 1,420°C (2). Once this temperature was reached, the chemical composition was checked. After the necessary corrections of the chemical analysis, a thermal analysis was performed to determine the liquidus temperature (=TL) of the melt. At a temperature of 200°C above TL, the melt was tapped into the ladle and simultaneously inoculated to the casting stream (3). The entire amount of inoculant was added in the first third, as the turbulence of the incoming melt allowed the inoculant to spread and mix well. After the required 16 kg had been

Figure 2

**Scanning electron microscopy (SEM) image (300x backscattered electron (BSE) detector) and determined phases via x-ray diffraction (XRD) and measured precipitation temperatures via DSC of Material 1 according to Reference 5.**

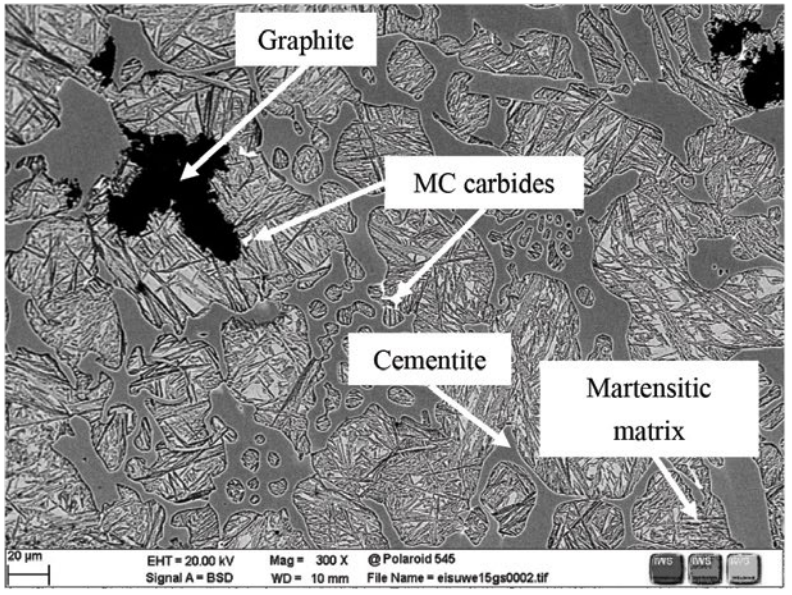


LOM+SEM/BSE+EDX:

- 2.45% Graphite
- 33.4% total carbides
- Nb-rich carbides
- Martensite

XRD:

- Martensite
- Austenite
- Cementite

DSC (peak temperatures):

- 1221°C (Austenite)
- 1126.4°C (MC-Carbides)
- 1121.8°C (Cementite)

Figure 3

Phase fraction diagram of Material 1.[5]

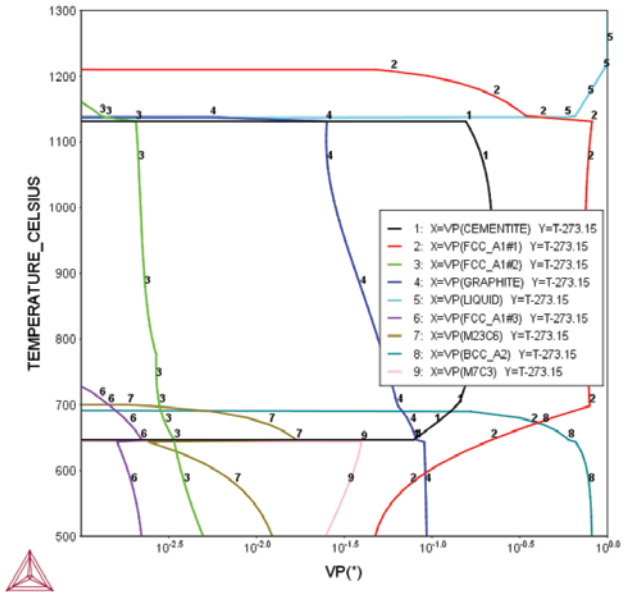


Figure 4

Isopleth for Material 1.[5]

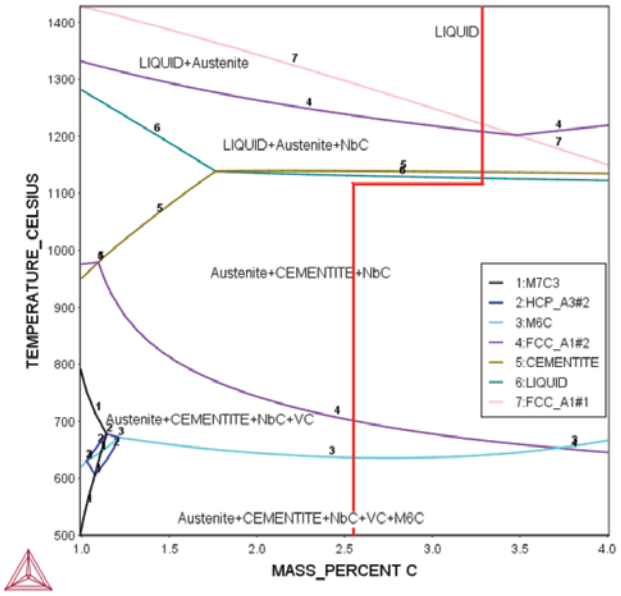


poured into the ladle and the inoculant had dissolved, a final sample was taken, and the temperature was continuously monitored (4). Due to the small tapping quantity (16 kg), the ladle was preheated to 700°C to prevent rapid cooling of the melt. At a defined temperature above TL, the melt was poured into a sand mold (5). Immediately after casting, the mold was covered with vermiculite to prevent rapid cooling of the mold (6). For each melting trial, three samples of 16 kg each were poured. After cooling to room temperature, the samples were removed from

Figure 5

Schematic pictures of the lab casting.

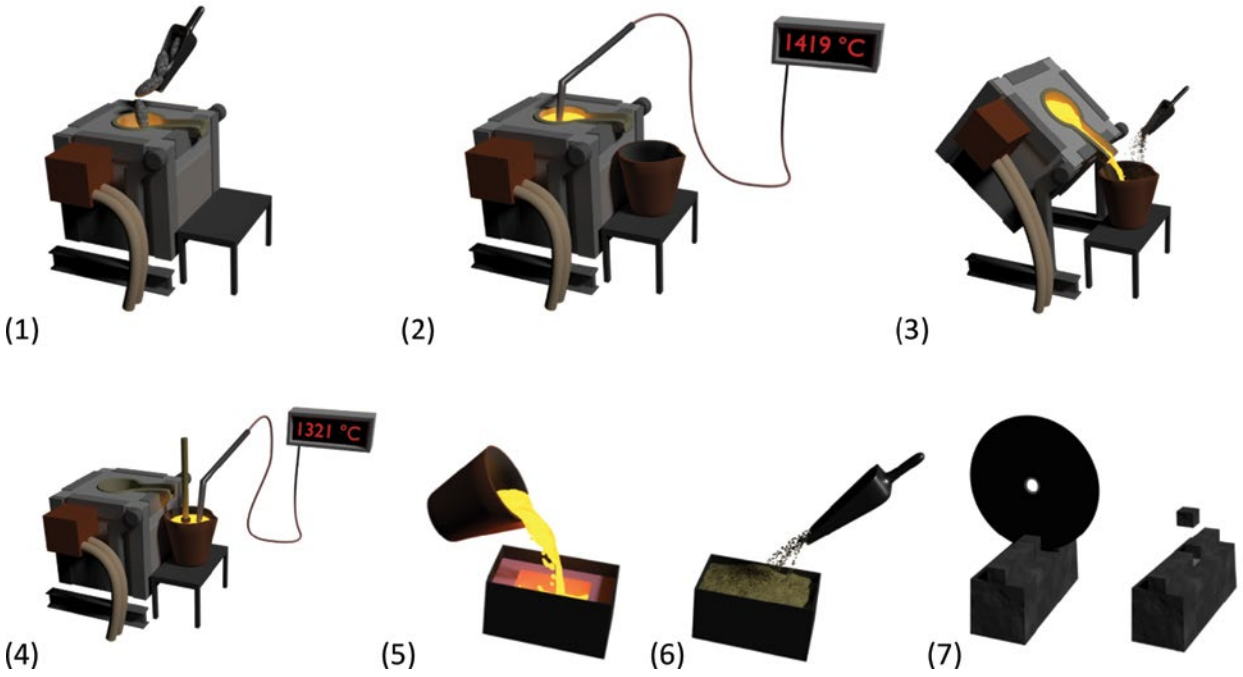

Figure 6

**Areas for the graphite and carbide measurement.**

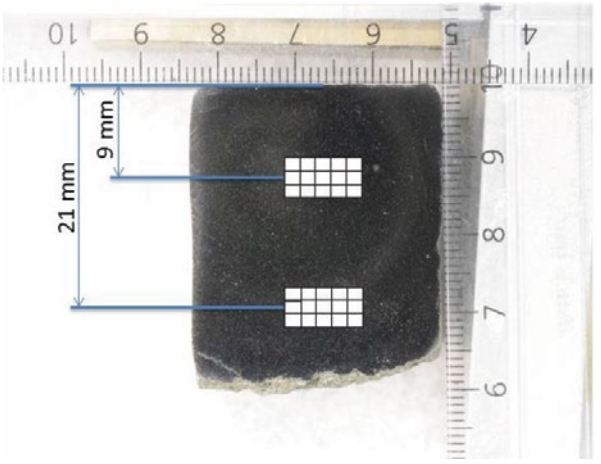


the molds. A disc cutting machine was used to make two cuts (7), then the sample was knocked out. These samples were first ground, lapped and finally polished for analysis.

For the examinations, only one part of the sample, taken from the center, was analyzed. The graphite and carbide content were determined using a light microscope model Zeiss Axio Imager M2m and the evaluation software ZEN Blue. The graphite content was measured at two different distances (9 and 21 mm) from the casting surface. For each measurement point, 15 individual images were taken at a 50x magnification (1,310.72 x 983.04 µm) and analyzed by the software. This corresponds to an examined area of approximately 4 x 5 mm at depths of 9 and 21 mm, as shown in Fig. 6.

On the unetched sample, graphite appears black under the light microscope, while everything else appears white. The software analyzes the "black" portion area-percentage-wise for each image, then sums up the 15 values and calculates the average. This value corresponds to the graphite content at 9 mm and 21 mm. Additionally, the particle density and shape factor were determined. The same procedure on the Nital etched sample was done to get the amount of carbides.

## Scale-Up Process

If the comparison of the microstructure of the lab casting with the thermodynamic calculated values led to a positive characterization, a large-scale test was planned. For this purpose, a centrifugal casting mold was prepared and only a shell was cast (see Fig. 7). The resulting sleeve was then sampled, examined and compared with the results from the laboratory tests.

In addition to the graphite and carbide measurement via light optical, quantitative image analysis and SEM examinations are also carried out at this stage. A Vega 3 SEM equipped with an Oxford Instruments Ultim® Max 170 energy-dispersive x-ray (EDX) system with two silicon drift detectors (SDD) of 200 mm² was used. An acceleration voltage of 30 kV, a beam intensity of 14, three frames and 300 µs detection time per pixel were used for the investigations. Phase analyses were performed using the SEM, which are schematically explained in Figs. 8 and 9. Fig. 8 shows the microstructure of a graphitic high-speed steel. The BSE micrographs, obtained by backscattered electrons, highlight a tempered martensite matrix (light gray area) surrounded by a high fraction of carbides (dark

Figure 7

**Casting of a sleeve in the foundry.**

Figure 8

BSE images of a graphitic high-speed steel (HSS) grade.

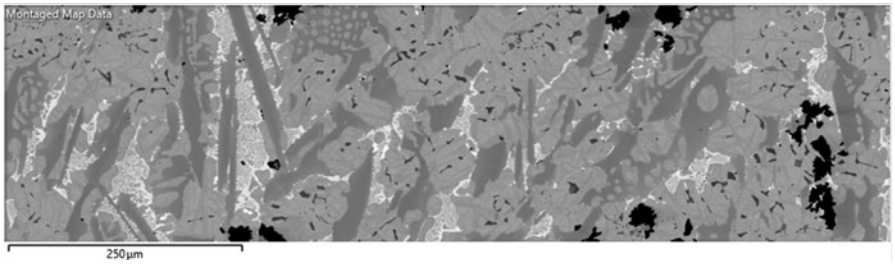


Figure 9

Energy-dispersive x-ray (EDX) analysis of BSE images of a graphitic HSS grade.


Figure 10

Schematic of the roll manufacturing process at ESW including (1) horizontal centrifugal casting, (2) assembly of the molds, (3) pouring of the core material and (4) sketch of a roll with shell and core material.

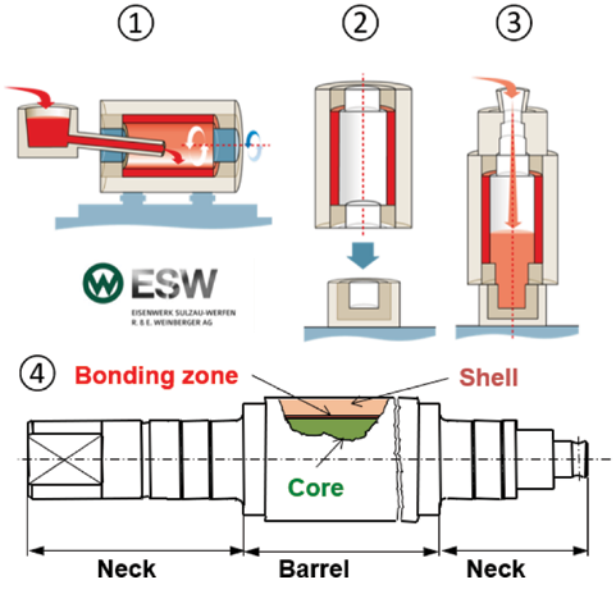


gray and white areas) and graphite particles (black particles).

The different gray scales of carbides correspond to different chemical compositions, darker phases consist of more elements with lower atomic mass, brighter phases consist of heavier elements.

The EDX analyses carried out on the same frames as reported in Fig. 8 confirmed the presence of cementite (turquoise), graphite (dark gray), Nb-based (green) and V-based (red) MC as well as Mo-based (yellow) M2C/M6C carbides for each grade, as indicated in Fig. 9.

If all investigations and characterizations prove to be promising, the next step can be taken, the casting of a prototype roll.

## Prototype Roll

Cast compound work rolls are mostly produced using the centrifugal spin-casting process. The melt for the shell is poured into a rotating mold and the centrifugal forces distribute the melt on its inner surface. After solidification of the shell, the so-called core iron is poured into the assembled mold and creates a permanent bonding between the shell and the core material as shown in Fig. 10.

## Wear Testing

The already well-established customary-designed two-roll test rig from ESW located at TU-Graz was modified with a third roll for simulating the backup rolls typically used in hot rolling mills, as shown in Fig. 11. In addition, a load-sensing and control system was implemented, which keeps the contact force between the load roll and the test roll constant during testing. The testing parameters including rotation of the rolls (i.e., slip between the rolls) and temperature of the load roll were predefined via intuitive visual touchscreen at the control unit. During each test run, the parameters were continuously recorded with a frequency of 1 Hz.

The test roll consisting of the material to be investigated was fixed to the upper driveshaft. The inductively heated load roll, simulating the strip/slab, was fixed to the lower driveshaft. The backup roll is undriven. The surface temperature of the heated load roll is continuously measured during wear testing using a pyrometer. Based on this measurement, inductive heating was controlled to maintain the constant surface temperature of the roll.

Figure 11

**Three-roll testing configuration TU-Graz (left) and at CRM Group (right).**

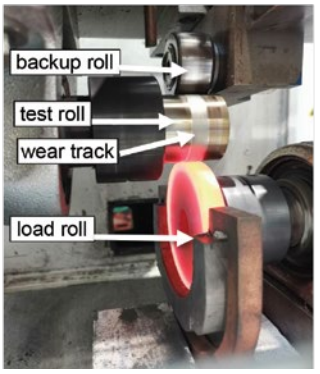


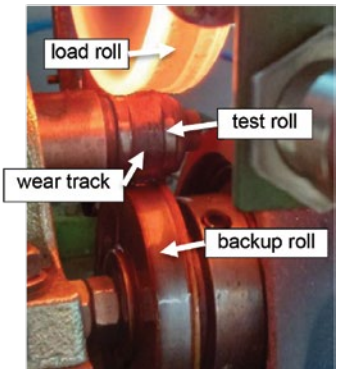


| Test rig at TU-Graz | | Test rig at CRM Group |
|---|---|---|
| 20–900°C | Temperature | 20–1,150°C |
| -30–30% | Slippage | 0–7% |
| Max. 1,250 MPa | Contact pressure | Max 1,500 MPa |
| Pressured air and lubrication | Cooling | Cooling water (different compositions) |

The contact force applied between the rolls was calculated according to the Hertzian contact theory.[10] Details about calculating the contact force by considering the specific roll dimensions and the setup of the test rig are described in References 8 and 9. During testing, the actual force was continuously measured using a load cell and adjusted using a pneumatic cylinder acting on the upper drive unit. Therefore, the contact force between the load roll and the test roll was virtually constant during each test run. Wear testing was performed at load roll temperatures between 150°C and 900°C. Slip of 0–12% between the test roll and the load roll was applied. The nominal contact pressures were 1,000 MPa between the test roll and the load roll and 1,250 MPa between the test roll and the backup roll. These testing parameters were based on on-site measurements performed at Tata DSP plant. As the parameters were controlled during testing, they can reasonably be assumed as constant. Wear tests were also conducted using CRM Group's rolling simulator[11] in order to evaluate the influence of cooling water (corrosion) on work roll degradation. The most significant differences between the two rigs are listed in Fig. 11.

After testing, each roll was sectioned. One of the cross-section surfaces was polished, whereas the wear track was investigated in as-tested condition (Fig. 12).

To analyze both the worn surface and the polished cross-section, each sample was tilted, as shown in Fig. 12. In each micrograph, the border between the worn surface and the polished cross-section was marked with an orange line. For evaluating the wear behavior, the worn surface as well as the microstructure beneath the surface must be considered. Based on these measurements, the maximum wear depth was determined at the center of each wear track after each test run.

Figure 12

**Setup for microstructure investigations using the 3D digital microscope and the SEM.**

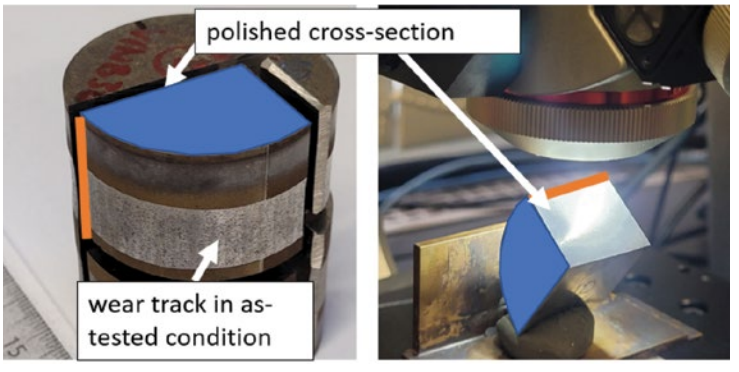


## On-Site Investigation at Tata DSP and Evaluation of the Performance

The roll surface was analyzed using a special light microscope for the examination of roll surfaces. Fig. 13 shows the setup used in the roll shop of the DSP mill. Micrographs are taken of the roll surface either after cleaning (degreased surface) or after a light 5% Nital etching to remove surface oxides formed during hot rolling.

## Results and Discussion

A total of 78 variants were calculated by using Thermo-Calc, which were carried out in collaboration with the FH-Wels. After this theoretical phase, 42 variants were cast in the lab. In parallel, eight selected variants were cast as a sleeve in the foundry. A total of 15 prototype rolls

Figure 13

Roll surface analysis in the DSP.

were cast, contributing to the further development and practical application of G-HSS technology. This multifaceted approach included both theoretical calculations and practical applications to improve the understanding and implementation of G-HSS in various fields. The results of the wear measurement process are explained in more detail in this section, focusing on the collaboration with CRM Group, Graz University of Technology, and the University of Trento. The aim of this joint initiative was to conduct a deep analysis of wear characteristics and patterns that provided deeper insights into the performance and durability of the materials involved.

The collaboration with Tata DSP and CRM Group in the field of on-site investigation and performance evaluation was of great importance. This partnership has enabled an in-depth analysis of performance metrics and ensured a thorough evaluation of the practical impact of the materials developed. The joint efforts with Tata DSP have provided valuable data on how the materials perform under real-world conditions, increasing the applicability and reliability of the research results. This collaborative approach underlines the commitment to not only theoretical innovations but also to practical solutions in the field of materials science and engineering.

## Wear Testing

At 150°C, the main driver for the wear resistance is cementite; the MC and $M_2C/M_6C$ carbides play a less dominant role. The maximum wear depth decreases with the total amount of cementite. Version 31 with the lowest fraction of cementite shows the highest wear depth. At relatively low contact temperature, under poor oxidizing conditions, the presence of an extended eutectic carbide network improves the load-bearing capability of the roll surface, causing lower wear. An adhesive wear mechanism is established, and the influence of carbide hardness is less. At high contact temperatures (750°C and 900°C), the formation of protective oxide layers is more evident, and the influence of the carbide type becomes more important with respect to hardness and oxidation behavior. While at 150°C the wear depth increases with higher fraction of MC and $M_2C/M_6C$ carbides (i.e., higher amount of cementite), at 750°C and 900°C the maximum wear depth decreases with increasing fraction of MC and $M_2C/M_6C$ carbides. At high temperatures, the hardness of the metallic matrix is relatively low (compared to 150°C) and the preferential wear of the matrix is more pronounced. Oxidation, compaction and sintering of the wear debris leads to the formation of compact oxide layers on the matrix. However, the hardness of carbides, especially MC and $M_2C/M_6C$, is higher than those of the metal matrix and the oxides. However, carbides clearly protrude from the contact surface and impede the formation of smooth wear surfaces. In this sense, the greater influence of hard carbides at higher temperature can be explained and it can be concluded that a certain content of MC and $M_2C/M_6C$ is fundamental for achieving sufficient wear resistance. The tests at 900°C show a slightly better wear behavior. The surface roughness of the worn surfaces clearly increases by increasing the contents of MC and $M_2C/M_6C$. Hence, the formation of sharper surface protrusions in grades containing only MC and $M_2C/M_6C$ impedes the formation of smooth contact surfaces and causes a stronger deterioration of the surface finish at high temperature. This is a very decisive aspect for rolls mounted in the last finishing stands of hot rolling mills. This effect is particularly important for MC, which shows higher oxidation tendency compared to $M_2C/M_6C$. Cementite shows less oxidation tendency compared to MC and $M_2C/M_6C$, but the lower hardness of this carbide reduces surface protrusions, which results in smoother wear surface profiles. The difference in wear depth between the grades can be clearly seen after the run-in period. At elevated temperatures, the alloy V19, which contained only a low fraction of MC and $M_2C/M_6C$, showed less wear resistance but better surface finishing (lower surface roughness) than grades V17 and V31. Hence, lower fractions of MC and $M_2C/M_6C$ and higher fractions of cementite are generally beneficial regarding the surface finish of the rolls.

A balance between MC, $M_2C/M_6C$ and cementite is needed to achieve less wear and to avoid unwanted oxidation behavior during hot rolling. Generally, microchipping and microcracking must also be considered, where cementite structures show disadvantages.

## On-Site Investigation at Tata DSP

**Stand F3:** The main actuators for roll degradation in stand F3 are thermal fatigue, contact fatigue and corrosion. Wear cannot be assessed through surface examinations, thus cannot be excluded from the mechanisms. Two versions were analyzed and compared in stand F3: V31 and V19. Although the rolled steel grade and campaign

length were very different between both materials, the following observations were made. V31 has a very rough surface, is highly oxidized, and seems sensitive to oxidation and to corrosion by the cooling water. V19, although analyzed after a very short campaign (8 wear km) and rolling an electrical steel grade (very abrasive compared to low carbon steel), shows a very smooth surface aspect, and several stuck strip oxide particles were observed on the roll surface. The surface oxidation of this material is low, and carbides can still be clearly seen.

**Stand F4:** Roll degradation in stand F4 follows the same mechanisms compared to stand F3 but all to a lesser extent. Rolls from two campaigns were analyzed. Compared to the reference version, V19 has a relatively similar surface degradation, although slightly rougher. Contact fatigue and thermal fatigue are, however, slightly lower on V19. V17 and a roll from a second competitor both behave similarly but with increased surface degradation compared to the reference or to V19. This is most likely linked to higher sensitivity to oxidation/corrosion of these roll materials.

**Stand F5:** In stand F5, 11 rolls were analyzed. The degradation mechanisms that are highlighted are contact fatigue and corrosion (wear cannot be assessed). Contrary to earlier stands, no thermal fatigue was observed on any roll out of stand F5. Version 19 keeps a very smooth surface aspect and a (very) thin oxide layer. Almost no degradation observed on this material. V19 has a similar trend to the special version but with slightly higher degradation and oxidation.

Several versions have been developed, delivered and are currently in use at DSP to collect process data. Ongoing evaluation focuses on overall roll performance, surface quality and wear compared to the standard version.

## Evaluation of the Performance

These results provide insight into the potential impact of different carbide types and quantities on surface quality. An increase in the volume fraction of MC and $M_2C/M_6C$ carbides in the microstructure contributes to increased wear resistance, which leads to improved rolling performance. However, this also leads to a higher surface roughness after the rolling campaign. This is due to the different oxidation, significantly higher hardness, and better wear resistance of MC and $M_2C/M_6C$ carbides compared to matrix and cementite carbides. As MC carbides are embedded in the matrix, the profile of the roll surface has more tips after the rolling campaign, which contributes to the development of an orange peel effect on the worn surface. The progression of the orange peel effect over the three-year project is shown in Fig. 14. The severity of orange peel, as measured by the Parsytec strip surface inspection system cameras, is shown in the graph for values greater than 2 (≥2) on the SH scale. From January 2021, various measures were implemented, and new tailor-made grades were introduced at the DSP plant. The introduction of V19 is considered a breakthrough. This graphitic HSS variant was tested in spring 2021 and showed a low orange peel formation. In post-summer 2021, mainly the standard version was used, which led to an increase in orange peel.

In contrast to the results of V19, V31, although labeled as "highly wear resistant," showed an unpleasant orange peel effect that did not meet the critical requirements for the strip surface. The results of the different grades are shown in Fig. 15.

Fig. 15 illustrates the wear, with the measured length plotted along the X-axis (corresponding to the Z-axis of the grinding machine). The profile measurement initiates 100 mm away from the edges of the work rolls.

Figure 14

**Progression of the orange peel effect over the three-year project.**

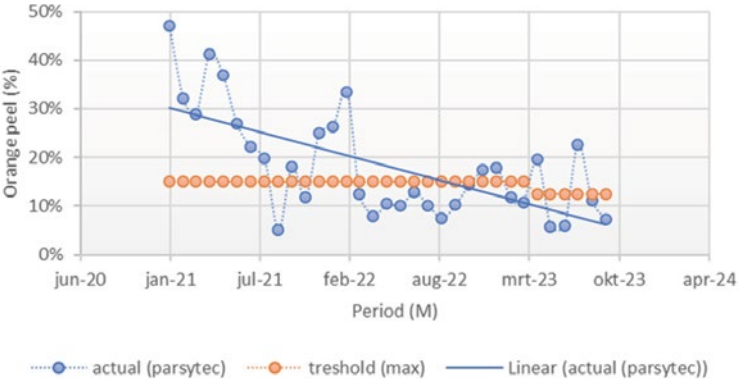


Figure 15

**Comparison of wear profile of the tested versions.**

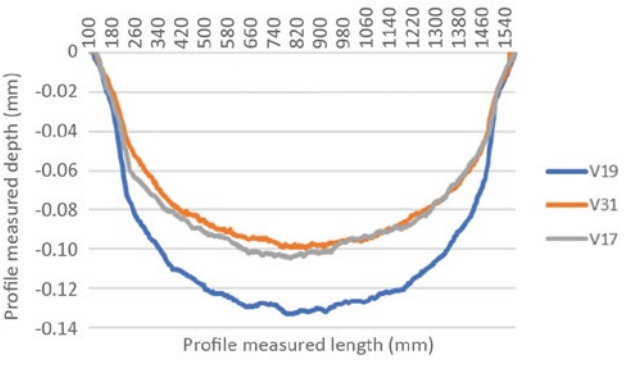

Considering the work roll width of 1,680 mm, the effective measured width is 1,480 mm (calculated as 1,680 – 2 * 100), with a resolution of 5 mm.

The total wear was summed up by dividing the rolled kilometers and then normalized for comparison to 10 km of rolled wear for each version grade. Fig. 15 clearly indicates that the macroscopic wear of V19 is the highest, whereas V31 demonstrates excellent performance and exhibits the best wear resistance among all three versions. From this, it can be concluded that the performance comparison of macroscopic mill wear aligns with the trends observed in the pilot mill trials conducted in the project at the Graz University of Technology.

## Conclusions

The success of this project is inextricably linked to the joint efforts and partnerships. The collaboration between research institutions such as University of Applied Sciences Upper Austria, CRM Group, Graz University of Technology and the University of Trento, as well as the cooperation with Tata DSP, has been crucial in achieving important milestones. The extensive research on G-HSS variations, wear measurement analysis and on-site investigations have not only broadened the understanding of materials science but have also produced practical applications in various industrial contexts.

The strength of this project lies in not only the theoretical calculations and laboratory-scale experiments, but also in the validation and performance evaluation in practice, which was made possible by the cooperation partners. The collaboration between these institutions was the keystone of the project's success and demonstrates the importance of sharing knowledge, expertise, and resources to push the boundaries of materials research. Thanks to this effective collaboration, the project was able to bridge the gap between theory and application and make progress in the development of high-performance materials for industrial applications.

## Acknowledgments

The authors would like to thank the Austrian Research Promotion Agency for the financial support of this work. Thanks also goes to the project partners University of Applied Sciences Upper Austria, Wels, Graz University of Technology and the University of Trento as well as CRM Group for the deep insights into their processes and for several fruitful discussions.



### References

1. K. Yamamoto and K. Ogi, "The Analysis of the Solidification Process of Abrasion Resistant Cr-V Cast Iron by the Use of Thermo-Calc," *Proceedings of the 65th World Foundry Congress,* 2002.
2. M. Pellizzari, "Thermodynamic Modeling for the Alloy Design of High Speed Steels and High Chromium Cast Irons," *Materials and Technology,* Vol. 44, No. 3, 2010, pp. 121–127.
3. H. Qu, B. Liao, L. Liu, D. Li, J. Guo, X. Ren and Q. Yang, "Precipitation Rule of Carbides in a New High Speed Steel for Rollers," *CALPHAD: Computer Coupling of Phase Diagrams and Thermochemistry,* Vol. 36, 2012, pp. 144–150.
4. A. Sommerfeld, "Investigations Into Graphite Nucleation in GJL Melts," (in German) dissertation, Technische Universität Clausthal, 2010.
5. A. Paar, L. Elizondo, M. Brandner, T. Trickl, B. Sonderegger, C. Béal and C. Sommitsch, "Application of Thermo-Calc TCFE7 to High-Alloyed Mottled Cast Iron," *Proceedings Thermec,* 2016.
6. G. Pöckl, Carbide Refinement and Non-Metallic Inclusions in Ledeburitic Tool Steels, Especially High-Speed Steels" (in German), dissertation, Montanuniversität Leoben, 2000.
7. K.H. Ziehenberger, "Alloying Improvement of Cast High-Speed Steel Rolls for Hot Strip Mills" (in German), dissertation, Technische Universität Wien, 2002.
8. J. Domitner, T. Stern, A. Leitner, M. Aigner, A. Paar, T. Trickl, L. Elizondo and C. Sommitsch, "Design of a Roll Test Bench for Investigating Thermo-Mechanical Wear," *Proceedings of the 11th Int. Tooling Conference,* RWTH Aachen, Aachen, Germany, 2019, p. 27.
9. J. Domitner, M. Aigner, T. Stern, A. Paar, C. Sommitsch, L. Elizondo, "Thermomechanical Wear Testing of Metal Matrix Composite Cladding for Potential Application in Hot Rolling Mills," *Steel Res. Int.,* Vol. 91, No. 5, 2020, 2070051.
10. H. Hertz, Ueber die Berührung fester elastischer Körper, J. Reine Angew, *Math.* 92, 1882, pp. 156–171.
11. G. Walmag, J. Malbrancke J. Sychterz, A. Brown, S. Mul and E. van den Elzen, "Laboratory and Pilot Mill Scale Evaluation Methods for Evaluating New Work Roll Grades Incorporating NDT Methods," *Proceedings of the Rolls 5 Conference,* Birmingham, United Kingdom, 2015.

AISTech This paper was presented at AISTech 2024 — The Iron & Steel Technology Conference and Exposition, Columbus, Ohio, USA, and published in the AISTech 2024 Conference Proceedings.